Density functional study of surface forces in athermal polymer solutions with additive hard sphere interactions: Solvent effects, capillary condensation, and capillary-induced surf...

ARTICLE *in* THE JOURNAL OF CHEMICAL PHYSICS · JULY 2002

Impact Factor: 2.95 · DOI: 10.1063/1.1486445

3 AUTHORS, INCLUDING:

Jan Forsman
Lund University
89 PUBLICATIONS **1,064** CITATIONS

SEE PROFILE

Density functional study of surface forces in athermal polymer solutions with additive hard sphere interactions: Solvent effects, capillary condensation, and capillary-induced surface transitions

Jan Forsman, Clifford E. Woodward, and Ben C. Freasier
School of Chemistry, University College, University of New South Wales, Australian Defence Force Academy, Canberra ACT 2600, Australia

(Received 31 January 2002; accepted 26 April 2002)

A density functional theory for polymer solutions is generalized to cases where the monomers have a different diameter to the solvent. An appropriate free energy functional is obtained by integration of the generalized Flory equation of state for such systems. This functional predicts that entropic demixing may occur in polymer solutions in which the solvent particles are smaller than the monomers. Demixing is promoted not only by a large size disparity, but also by a high pressure as well as by polymer length. The existence of two separate phases in the bulk solution suggests the possibility of capillary-induced phase transitions, even when the confining surfaces are hard, but otherwise inert. We examine such phase transitions and their relation to surface forces and colloidal stability. The density functional theory also predicts that under certain conditions, layering transitions will occur at hard and flat surfaces. A transition from a thin to a thick polymer-rich surface layer may take place as the separation between two surfaces is decreased, and we study the concomitant change on the surface force. Stable thick phases are predicted even at very large undersaturations, and they give rise to a profound increase of the range and strength of the surface force. We furthermore include comparisons with predictions from a model in which the solvent only enters the description implicitly. Responses of the surface forces to changes in monomer diameter, solvent diameter, polymer density, and chain length are investigated. [DOI: 10.1063/1.1486445]

I. INTRODUCTION

Polymers are often used to regulate the stability of colloidal systems, and several experimental[1–8] and theoretical[9–24] studies have provided at least a qualitative description of how this is achieved. Surface force experiments, complemented by simulations of polymers in confined geometries, have been instrumental in improving our understanding of how polymer molecules affect the interaction between particles of colloidal dimensions.

Even so, some fundamental features still remain unresolved. The most important of these is probably the experimentally observed[3,5,13] restabilization that prevents flocculation of colloidal dispersions from occurring when the polymer concentration is relatively high. Early mean-field and scaling analyses[12,15,18] predicted a monotonic attraction, irrespective of polymer concentration. However, improved mean-field theories[22] as well as simulations[17,23,24] and packing considerations[20,25] have supported the possibility of a repulsive regime. The question of whether such a repulsion would provide a true thermodynamic or mere kinetic stabilization is yet another unresolved issue.

In most theoretical treatments of polymer solutions, the solvent enters the description implicitly. Borrowing ideas from Flory-Huggins theory, it merely contributes to the ''effective'' interaction between monomers. In a poor solvent, monomers effectively attract each other, and in a good solvent, the effective interaction is repulsive. This model is simple and appealing. Nevertheless, in many circumstances it may be a poor description of a system where the major constituent is the solvent. For example, fundamental thermodynamic phenomena, such as binary phase equilibrium, are not included in such a coarse-grained model. In this work, we will use density functional theory (DFT) to study surface forces in polymer solutions wherein the solvent particles are treated *explicitly*. In order to reduce the number of variable parameters, we have restricted ourselves to athermal polymer solutions confined between flat hard walls.

Several different DFT versions for polymeric systems have been proposed[26–31] with subsequent further developments.[32–36] An important aspect of these latter theories is that they contain a nonlocal treatment of excluded volume effects. This nonlocality, which was originally introduced by Nordholm and co-workers in the *generalized van der Waals* theory of simple fluids,[37] admits an accurate description of packing effects.

The polymer density functional theory of Woodward[28] has the same structure as the generalized van der Waals theories: i.e., an equation of state enters the theory explicitly. Connectivity is properly included in the sense that for ideal chains the theory is exact. Even with a very simple equation of state, the theory is able to predict structural properties and surface forces for athermal polymer melts and solutions with surprisingly high accuracy.[19,28] Woodward and Yethiraj[34] improved the functional by adopting the generalized Flory-dimer (GFD) equation of state,[38–40] which has been shown to be to be very accurate when compared with simulations of

short athermal polymers.[39,41] In this study, we will extend the theory further by utilizing a generalization of the GFD equation of state to polymer solutions in which the spherical solvent and monomer particles have different diameters. The size asymmetry is characterized by the diameter ratio $q=\sigma_s/\sigma_m$, where σ_m and σ_s are the monomer and solvent sphere diameters, respectively. An equation of state for such systems, henceforth denoted the *extended* GFD, was developed a few years ago by Wichert *et al.*[42] It accurately predicts the compressibility for a large range of diameter ratios and polymer lengths. Other equations of state for these systems have also been suggested, with similar performance.[43–47] However, the extended GFD equation of state has the advantage that the compressibility is expressed in terms of the total volume fraction with coefficients that are independent of the total density. This facilitates the development of a corresponding free energy functional. Our aim is to obtain qualitatively and semiquantitatively correct predictions, and for this purpose the extended GFD equation of state appears eminently suited.

Recent theoretical investigations on binary mixtures of hard spheres with different diameters[48–58] indicate that an entropy driven demixing transition may take place in these systems. Recent experimental work on mixtures of colloidal spheres[55,59–63] supports these findings. The theories predict that the transition does not occur unless there is a rather large size disparity between species, $q\approx 0.2$ or less. The transition has proved difficult to describe. For example, even qualitative predictions by integral equation theories are sensitive to the choice of closure.[48,64,65] Indeed, the existence of this transition has also been disputed.[65,66] Most studies to date predict that one or both coexisting phases will be a solid. Recently, however, Henderson *et al.*[57] have suggested that stable fluid-fluid equilibria may exist when the concentration of the large spheres is very dilute. The physical origin of the transition is generally attributed to a depletion mechanism,[9] whereby large spheres at high density will expel smaller spheres and be compressed by the surrounding bulk pressure.[9,20,48,50,53]

We conjecture that a similar type of phase transition exists in athermal polymer solutions, provided the diameter ratio q is small enough. We shall apply the extended GFD equation of state to demixing in bulk athermal polymer solutions, as well as consider the consequences of possible phase transitions on surface forces.

The article is organized as follows: In Sec. II we describe the polymer model and the density functional theory for polymer solutions in which the solvent diameter differs from that of the monomers. We present and interpret the results in Sec. III and finalize with a short summary of our major conclusions in Sec. IV.

II. THEORY

The general structure of the polymer density functional theory has been described elsewhere.[19,28] We shall briefly recapitulate its basic features, but we will focus on the novel part: namely, its extension to solutions in which the diameter of the solvent particles differ from that of the monomers.

Consider a polymer made up of r monomers. Denoting the coordinate of monomer i by $\mathbf{r}_i$, we can represent a polymer configuration by $\mathbf{R}=(\mathbf{r}_1,\ldots,\mathbf{r}_r)$. The total bonding potential connecting adjacent monomers in the chain, $V_b(\mathbf{R})$, contains no angular part and the distance between adjacent monomers is fixed to the hard sphere diameter σ_m, i.e.,

$$e^{-\beta V_b(\mathbf{R})}\propto\prod\ \delta(|\mathbf{r}_{i+1}-\mathbf{r}_i|-\sigma_m), \tag{1}$$

where $\beta=1/(k_BT)$ is the inverse thermal energy. This means that each monomer can move freely on the spherical surfaces formed by the monomers to which it is bonded. This defines the so-called freely jointed pearl-necklace polymer model. We denote the multipoint polymer density distribution by $N(\mathbf{R})$: i.e., $N(\mathbf{R})d\mathbf{R}$ is the number of polymer molecules having configurations between $\mathbf{R}$ and $\mathbf{R}+d\mathbf{R}$. Let us start by restricting the treatment to pure polymer fluids. In absence of external fields, we can write the exact expression for the ideal entropy functional $\mathcal{F}_p^{\mathrm{id}}$ as[28]

$$\beta\mathcal{F}_p^{\mathrm{id}}=\int N(\mathbf{R})\{\ln[N(\mathbf{R})]-1\}d\mathbf{R}+\beta\int N(\mathbf{R})V_b(\mathbf{R})d\mathbf{R}. \tag{2}$$

The monomer density $n_m(\mathbf{r})$ is given by

$$n_m(\mathbf{r})=\int\sum_{i=1}^{r}\delta(\mathbf{r}-\mathbf{r}_i)N(\mathbf{R})d\mathbf{R}. \tag{3}$$

Following Woodward,[28] we approximate the excess (hard sphere) entropy F_p^{ex} of the pure polymer fluid in terms of the monomeric density:

$$F_p^{\mathrm{ex}}\approx\int a_m^{\mathrm{ex}}[\overline{n}_m(\mathbf{r})]n_m(\mathbf{r})d\mathbf{r}, \tag{4}$$

where a coarse-grained monomer density $\overline{n}_m(\mathbf{r})$ is defined as

$$\overline{n}_m(\mathbf{r})=\frac{3}{4\pi\sigma_m^3}\int_{|\mathbf{r}-\mathbf{r}'|<\sigma_m}n_m(\mathbf{r}')d\mathbf{r}'. \tag{5}$$

By formulating the excess entropy in such a nonlocal fashion, the functional is able to handle packing effects,[37] which, naturally, may be important in the heterogeneous systems we will investigate.

For a polymer *solution* the free energy also depends on the solvent density, and a general expression for the (approximate) grand potential Ω of a hard sphere polymer solution in absence of external fields can be written as[28]

$$\begin{aligned}\beta\Omega[N(\mathbf{R}),n_s(\mathbf{r})]=\beta\mathcal{F}_p^{\mathrm{id}}&+\int n_s(\mathbf{r})\{\ln[n_s(\mathbf{r})]-1\}d\mathbf{r}\\&+\int n_m(\mathbf{r})a_m^{\mathrm{ex}}[\overline{n}_m(\mathbf{r}),\overline{n}_s(\mathbf{r}),q]d\mathbf{r}\\&+\int n_s(\mathbf{r})a_s^{\mathrm{ex}}[\overline{n}_m(\mathbf{r}),\overline{n}_s(\mathbf{r}),q]d\mathbf{r}\\&-\beta\mu_p\int n_m(\mathbf{r})d\mathbf{r}-\beta\mu_s\int n_s(\mathbf{r})d\mathbf{r},\end{aligned} \tag{6}$$

where μ_p and μ_s are the polymer and solvent chemical potentials, respectively. As previously stated, the ratio between solvent and monomer hard sphere diameters is defined as $q \equiv \sigma_s/\sigma_m$. We denote the solvent density by $n_s(\mathbf{r})$, and the corresponding coarse-grained quantity $\overline{n}_s(\mathbf{r})$ is defined analogously to Eq. (5), with the index *s* replacing *m*. We will only consider polymer solutions with additive hard sphere interactions in this study: i.e., a monomer and a solvent particle will experience an interaction which is zero when they are separated by a distance exceeding $(\sigma_m+\sigma_s)/2$, while the interaction becomes infinite at separations below this threshold value. The hard sphere diameters relevant for monomer-monomer and solvent-solvent interactions are of course given by σ_m and σ_s, respectively. In order to proceed further, we need an approximation of the excess free energies per particle for monomer and solvent, $a_m^{\mathrm{ex}}[\overline{n}_m(\mathbf{r}),\overline{n}_s(\mathbf{r}),q]$ and $a_s^{\mathrm{ex}}[\overline{n}_m(\mathbf{r}),\overline{n}_s(\mathbf{r}),q]$. Woodward and Yethiraj have derived such expressions for polymer solutions in which the monomers and the solvent particles have equal diameters[34] by integrating the corresponding GFD equation of state.[40] We shall proceed along the same lines, but our starting point will be the extension of the GFD to mixtures where the solvent particle diameter differs from that of the monomers. An equation of state for such systems has been presented by Wichert, Gulati, and Hall (WGH).[42] We shall find our desired approximations of $a_m^{\mathrm{ex}}[\overline{n}_m(\mathbf{r}),\overline{n}_s(\mathbf{r}),q]$ and $a_s^{\mathrm{ex}}[\overline{n}_m(\mathbf{r}),\overline{n}_s(\mathbf{r}),q]$ by integrating their expression for the compressibility. WGH based their derivation on the so-called ''osmotic equation of state'' for the pressure *P*:

$$\begin{aligned}\beta P(x_p,\eta) = {} & \frac{x_p\eta}{\overline{v}}[1-\ln p_p(\eta,r,x_p,q)] \\ & + \frac{x_p}{\overline{v}}\int_0^\eta \ln p_p(\eta',r,x_p,q)\,d\eta' \\ & + \frac{x_s\eta}{\overline{v}}[1-\ln p_s(\eta,r,x_p,q)] \\ & + \frac{x_s}{\overline{v}}\int_0^\eta \ln p_s(\eta',r,x_p,q)\,d\eta', \end{aligned} \tag{7}$$

where x_p and x_s are the polymer and solvent mole fractions, while $p_i(x_p,\eta)$ denote the probability of a successful insertion of species *i* into the solution. Further, $\overline{v}$ is the molar average of the volume v_i of a molecule of species *i*, i.e., $\overline{v} = x_p v_p + x_s v_s$. If we denote the density of species *i* by ρ_i, the total volume fraction η is given by $\eta = (\pi/6)[r\rho_p\sigma_m^3 + \rho_s\sigma_s^3]$. The integrals are performed at a constant molar ratio, in order to ensure consistency with the Gibbs-Duhem relation for the mixture.[34]

WGH estimated $p_p(\eta,r,x_p,q)$ as

$$\begin{aligned} p_p(\eta,r,x_p,q) \approx {} & [p_d(\eta,r,x_p,q)]^{[Y_{\mathrm{mix}}(r,x_m,q)+1]} \\ & \times [p_m(\eta,r,x_p,q)]^{-Y_{\mathrm{mix}}(r,x_m,q)}, \end{aligned} \tag{8}$$

where p_d is the probability of inserting a dimer into the polymer solution, while p_m is the analogous quantity for a monomer. The factor Y_{mix} accounts for the reduction in excluded volume brought about by bonding. It depends on the polymer length, the ratio between solvent and monomer diameters, and the monomer molar ratio $x_m = r\rho_p/(r\rho_p+\rho_s)$. The explicit expression for Y_{mix} is given by WGH. In order to proceed further, WGH introduced yet another approximation by equating the dimer and solvent insertion probabilities with those obtained in the dimer-solvent mixture that would result if every second bond in the polymers were broken. Similarly, the monomer insertion probability was approximated with that in the monomer-solvent mixture obtained by breaking every bond in the polymers. These insertion probabilities were in turn derived from scaled particle theory.[67] We will not recapitulate the entire derivation by WGH. They presented a very general theory for binary mixtures of chains of different length. Since we will limit ourselves to a polymer solution, i.e., a mixture of solvent particles and polymers, we can simplify their notation considerably. We shall revert to the following simplified notation.

(i) $\mathfrak{R}_2$ indicates that the quantity $\mathfrak{R}$ relates to the insertion of a dimer into the hypothetical dimer-solvent mixture as described above. In the general nomenclature by WGH, this would be written as $\mathfrak{R}_{a_2}^{(2,1)}$, where the polymers are ''species *a*.''

(ii) $\mathfrak{R}_1$ indicates that the quantity $\mathfrak{R}$ relates to the insertion of a monomer into the hypothetical monomer-solvent mixture described above. This corresponds to $\mathfrak{R}_{a_1}^{(1,1)}$ in the notation by WGH.

(iii) $\mathfrak{R}_0$ indicates that the quantity $\mathfrak{R}$ relates to the insertion of solvent particles into the dimer-solvent mixture. WGH would write this as $\mathfrak{R}_{b_1}^{(2,1)}$, with *b* denoting the solvent.

We can use this simplified notation to write their expression for the compressibility as

$$\begin{aligned} Z = {} & x_p[(Y_{\mathrm{mix}}(r,x_m,q)+1)\zeta_2(\eta,x_m,q) \\ & - Y_{\mathrm{mix}}(r,x_m,q)\zeta_1(\eta,x_m,q)] + x_s\zeta_0(\eta,x_m,q), \end{aligned} \tag{9}$$

where

$$\begin{aligned} \zeta_i(\eta,x_m,q) = {} & -[1+\Upsilon_i(x_m,q)]\frac{\ln[1-\eta]}{\eta} - \frac{\Upsilon_i(x_m,q)}{(1-\eta)^3} \\ & + \frac{[\Phi_i(x_m,q)+2Z_i(x_m,q)-X_i(x_m,q)]\eta}{(1-\eta)^3} \\ & - \frac{\Phi_i(x_m,q)\eta^2}{(1-\eta)^3} + \frac{W_i(x_m,q)\eta^3}{(1-\eta)^3}, \end{aligned} \tag{10}$$

with

$$\Upsilon_i(x_m,q) = W_i(x_m,q) + Y_i(x_m,q) + 3Z_i(x_m,q) \tag{11}$$

and

$$\begin{aligned} \Phi_i(x_m,q) = {} & X_i(x_m,q)/2 + 5Y_i(x_m,q)/2 \\ & + 11Z_i(x_m,q)/2 + 3W_i(x_m,q). \end{aligned} \tag{12}$$

Expressions for the coefficients $W_i(x_m,q)$, $X_i(x_m,q)$, $Y_i(x_m,q)$, and $Z_i(x_m,q)$ are given by WGH. These depend on the monomer molar ratio, but not on the total volume fraction. If we now integrate Eq. (9) using the relation

$$f^{\mathrm{ex}} = \frac{1}{V}\int \frac{Z-1}{\eta}\,d\eta, \tag{13}$$

where V is the total volume and f^{ex} is the excess free energy per unit volume, we get

$$f^{\mathrm{ex}}=\rho_p\{(r-2)Y'_{\mathrm{mix}}(r,x_m,q)[a_2^{\mathrm{ex}}(\eta,x_m,q)-a_1^{\mathrm{ex}}(\eta,x_m,q)]+a_2^{\mathrm{ex}}(\eta,x_m,q)\}+\rho_s a_0^{\mathrm{ex}}(\eta,x_m,q), \tag{14}$$

with $Y'_{\mathrm{mix}}\equiv Y_{\mathrm{mix}}/(r-2)$, and

$$\begin{aligned}a_i^{\mathrm{ex}}(\eta,x_m,q)=&\frac{1-\eta}{\eta}\ln[1-\eta]+1+\Upsilon_i(x_m,q)\left[\ln[1-\eta]\left(\frac{1-\eta}{\eta}+1\right)-\frac{1}{1-\eta}-\frac{1}{2(1-\eta)^2}+\frac{5}{2}\right]\\&+[\Phi_i(x_m,q)+2Z_i(x_m,q)-X_i(x_m,q)]\left(\frac{1}{2(1-\eta)^2}-\frac{1}{2}\right)\\&+W_i(x_m,q)\left(\frac{1}{2(1-\eta)^2}-\frac{2}{1-\eta}-\ln[1-\eta]+\frac{3}{2}\right)+\Phi_i(x_m,q)\left(\frac{1}{1-\eta}-\frac{1}{2(1-\eta)^2}-\frac{1}{2}\right).\end{aligned} \tag{15}$$

The term proportional to $(r-2)$ in Eq. (14) is the contribution from interior monomers, while the end monomers provide the dimer excess free energy term. Collecting our results and adding external potentials $V_m^{\mathrm{ext}}(\mathbf{r})$ and $V_s^{\mathrm{ext}}(\mathbf{r})$ which act on monomers and solvent, respectively, we end up with the following expression for the grand potential:

$$\begin{aligned}\beta\Omega=\beta\mathscr{F}_p^{\mathrm{id}}+\int\{n_m(\mathbf{r})-n_e(\mathbf{r})\}\{Y'_{\mathrm{mix}}(r,x_m,q)[a_2^{\mathrm{ex}}(\overline{\eta}(\mathbf{r}),\overline{x}_m(\mathbf{r}),q)-a_1^{\mathrm{ex}}(\overline{\eta}(\mathbf{r}),\overline{x}_m(\mathbf{r}),q)]\}d\mathbf{r}+\tfrac{1}{2}\int n_e(\mathbf{r})a_2^{\mathrm{ex}}(\overline{\eta}(\mathbf{r}),\overline{x}_m(\mathbf{r}),q)\\\times d\mathbf{r}+\int n_s(\mathbf{r})a_0^{\mathrm{ex}}(\overline{\eta}(\mathbf{r}),\overline{x}_m(\mathbf{r}),q)d\mathbf{r}+\beta\int n_m(\mathbf{r})[V_m^{\mathrm{ext}}(\mathbf{r})-\mu_p]d\mathbf{r}+\beta\int n_s(\mathbf{r})[V_s^{\mathrm{ext}}(\mathbf{r})-\mu_s]d\mathbf{r},\end{aligned} \tag{16}$$

where $\overline{\eta}(\mathbf{r})=(\pi/6)[\overline{n}_m(\mathbf{r})\sigma_m^3+\overline{n}_s(\mathbf{r})\sigma_s^3]$ is the total coarse-grained volume fraction and $\overline{x}_m(\mathbf{r})=\overline{n}_m/(\overline{n}_m+\overline{n}_s)$ is the coarse-grained monomer molar ratio.

In this study, we will consider polymer solutions confined by hard planar walls. Defining the direction adjacent to the walls as z, symmetry allows the two remaining (x,y) dimensions to be integrated out, i.e., $\Omega=\Omega[n_m(z),n_s(z)]$. The external potentials are defined as

$$V_\alpha^{\mathrm{ext}}(z)=\begin{cases}\infty, & z<\dfrac{\sigma_\alpha}{2},\quad z>h-\dfrac{\sigma_\alpha}{2},\\[2ex] 0, & \dfrac{\sigma_\alpha}{2}\leqslant z\leqslant h-\dfrac{\sigma_\alpha}{2},\end{cases} \tag{17}$$

with $\alpha=s,m$. The relevant free energy of interaction per unit area, F_{int}, is given by the grand potential, corrected by a bulk pressure term:

$$F_{\mathrm{int}}[n_m(z),n_s(z)]=\Omega[n_m(z),n_s(z)]+P_b(h-\sigma_s), \tag{18}$$

where P_b is the bulk pressure. Defined in this way, F_{int} will approach twice the single-wall interfacial tension at large surface separations. When presenting our results, we shall often normalize F_{int} by subtracting off its value at the largest separation $h_{\max}$ we have considered. In that way, the free energy curves obtained under different conditions can more easily be compared. F_{int} was minimized using a Picard iteration scheme, as outlined by Woodward.[28] Since the density profiles we have obtained are rapidly varying near the walls, we had to use a relatively fine grid spacing in our calculations: $\delta z=0.01\sigma_m$. One important feature of this functional is that it is thermodynamically consistent in the sense that wall sum rules, such as the contact theorem,[68] are fulfilled. This means that since the GFD expression for the compressibility, Eq. (9), has been shown to agree very well with simulation data for a wide range of volume fractions and hard sphere diameter ratios,[42] the total contact density obtained from the density functional theory will also be accurate. Furthermore, confirming that the net interaction pressure P_{int}, as obtained via the relation $\beta P_{\mathrm{int}}=-\beta\,\partial F_{\mathrm{int}}/\partial h$, agrees with the total contact density subtracted by the single-surface contact density provides a good independent check of the calculation program. The former relation gives better accuracy for a given grid spacing, though, so all the net interaction pressure results we present have been obtained by a discrete differentiation of $F_{\mathrm{int}}(h)$.

With one exception, each symbol shown in the graphs we present below indicates a calculated datum point, while the lines are a guide to the eye. The exception is density profiles, where the data points are so dense that they are represented by lines directly.

III. RESULTS

A. Demixing in bulk solutions

In this section, we investigate the predictions of the extended GFD density functional when applied to athermal bulk polymer solvent mixtures. The monomers are assigned a larger diameter than the solvent particles. This can be considered a type of ''united atom'' model and is applicable to situations where the often complex internal structure of a polymer molecule can be approximated by a model of large bonded spheres.

The free energy functional predicts a demixing transition in these systems. Figure 1 shows the calculated critical volume fractions as a function of polymer length for a number of different size ratios. The models display equilibria at fairly modest volume fractions, where the fluid phase is expected to be stable. Indeed, we did not investigate the existence of

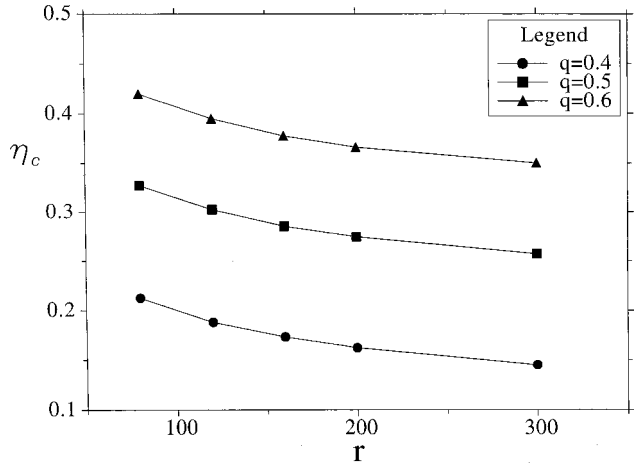

FIG. 1. Value of the total volume fraction η at the critical point of the bulk polymer solution versus the length r of the dissolved polymers. The three curves display different ratios q between solvent and monomer hard sphere diameters.

possible stable solid phases. Interestingly, we observe demixing even for relatively small size disparity, e.g., $q=0.6$. A specific example of a bulk coexistence curve is given in Fig. 2.

It appears evident that the presence of polymer molecules as one of the components of the mixture facilitates demixing. The larger monomer particles are brought together by the depletion attraction mechanism induced by the smaller solvent particles. This process is promoted by the fact that monomers are bound into chains, giving rise to a cooperative effect which increases the propensity of the system to undergo a phase transition. In a related finding, Anta *et al.*[65] showed, using integral equation theory, that the demixing transition in a mixture of hard dimers and smaller hard spheres occurs more readily than in the corresponding hard sphere mixture. There have also been some simulation studies of single polymers undergoing solvent-induced ''collapse'' transitions.[52,69,70] However, these results were obtained with the solvent being equal to[52] or considerably larger than[69,70] the monomers. This makes comparisons with our system less direct.

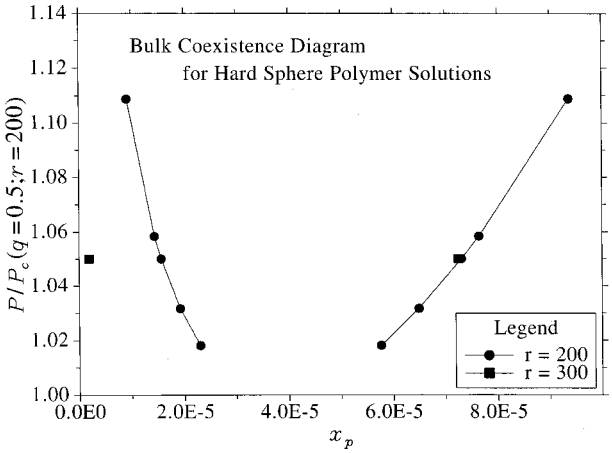

FIG. 2. Bulk coexistence curve for a 200-mer solution with $q=0.5$ (circles). The squares indicate corresponding coexistence values for the polymer molar ratio x_p in a 300-mer solution at a bulk pressure of $P_b/P_b^c(N=200, q=0.5)=1.05$, i.e., 5% higher than the critical pressure for the 200-mer solution. This corresponds to $\beta P_b \sigma_m^3 = 14.249\,55$.

The depletion mechanism enters the free energy functional via the scaled particle theory expressions for insertion of particles into mixtures (see previous section). In this respect, it contains a similar phenomenology to the treatment of hard sphere mixtures given by Lekkerkerker and Stroobants.[50] The cooperativity effect is implicitly included in the functional via the exact treatment of connectivity in the ideal contribution to the free energy. Though the functional was not specifically developed to describe demixing in polymer solutions, it would not be the first time where a simple but physically reasonable model is able to qualitatively account for phenomena to which it was not initially addressed. A well-known example is the van der Waals equation of state, which can be used to describe condensation, even though it was originally intended as an improved description of gases.

Confirmation of our prediction for demixing in the bulk could be provided by computer simulations. Unfortunately, very extensive computational resources would be necessary to obtain the simulation analogue of Fig. 1. This is beyond the scope of the present work. Instead, we conjecture that, given the reasonable approximations of the theory and the excellent accuracy obtained for bulk pressures, the prediction of demixing in these systems is plausible.

B. Surface-induced demixing

1. Capillary condensation

Henceforth, we shall denote the polymer-rich phase as either ''concentrated'' or ''condensed,'' while the polymer poor phase is termed ''dilute.'' The molar fraction of polymer in the bulk solution is denoted as x_p. Following from the discussion in the previous section, we expect that at very low values for x_p, the dilute phase is stable in the bulk solution. However, when the polymer molar fraction is increased, a demixing transition will eventually occur, provided the pressure is greater than its critical value for that solution. At a given pressure, we will by x_p^{sat} denote the polymer molar fraction in the dilute branch at bulk coexistence. If the ratio x_p/x_p^{sat} is less than unity, the bulk fluid is termed undersaturated.

The depletion attraction between monomers that brings about the demixing transition in the bulk fluid also exists between monomer particles and a hard wall. Thus a hard wall can favor demixing. Furthermore, if the solution is bounded by a pair of hard surfaces, then we may observe a capillary induced demixing or ''condensation'' of the polymer-rich (concentrated) phase between the surfaces.

We consider a polymer solution confined between hard walls in equilibrium with an undersaturated bulk solution at a reduced pressure of $\beta P_b \sigma_m^3 = 14.249\,55$. This pressure is 5% higher than its critical value for a bulk mixture containing hard spheres and 200-mers, with a diameter ratio of $q=0.5$. The distance between the surfaces is allowed to vary. At large separations the confined fluid will be in the dilute phase. As the separation is decreased, ''condensation'' to the

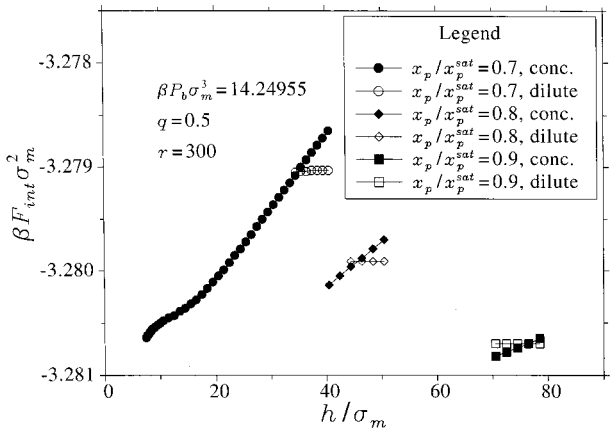

FIG. 3. Free energy of interaction, F_{int}, as a function of surface separation h, at three different degrees of undersaturation: $x_p/x_p^{\text{sat}}=0.7$ (circles), 0.8 (diamonds), and 0.9 (squares), for a 300-mer solution at $\beta P_b\sigma_m^3=14.249\,55$. Open symbols are dilute branch results, while the variation of F_{int} with separation is much more rapid in the concentrated branch (solid symbols). At each of these bulk polymer concentrations, this results in a crossing at $h\equiv h_{\text{cap}}$, where capillary condensation is predicted to occur.

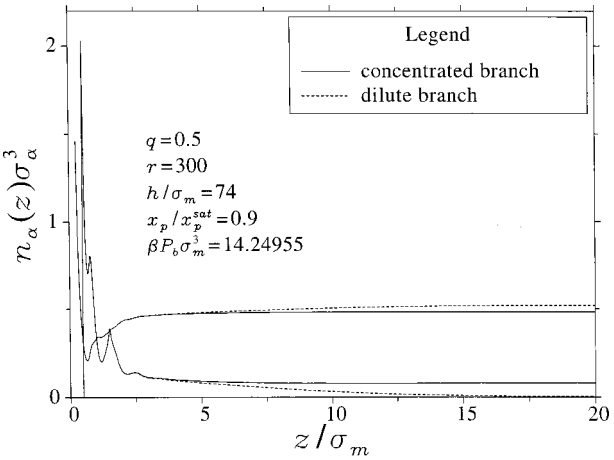

FIG. 4. Density profiles of concentrated (solid line) and dilute (dashed line) branches of 300-mer solutions at $h/\sigma_m=74$ and $x_p/x_p^{\text{sat}}=0.9$. The bulk pressure is $\beta P_b\sigma_m^3=14.249\,55$. The solvent density profiles can be identified by the fact that they are higher than their monomer analogue at large distances from the surface.

concentrated phase may occur. In Fig. 3, we have plotted the free energy of interaction per unit area, F_{int}, as a function of separation for a solution of 300-mers, at $q=0.5$, for a range of undersaturations in the bulk solution. It is apparent that two different branches exist, corresponding to concentrated and dilute phases. The functional predicts the existence of metastable portions on each branch. Coexistence occurs at that separation where the branches intersect. We denote this separation as h_{cap}. Clearly, h_{cap} decreases as the degree of undersaturation increases. Furthermore, due to cooperative effects, a solution containing longer polymers will display capillary condensation at a larger separation. Similarly, for a given chain length and pressure, h_{cap} increases as q decreases, at least in the vicinity of $q=0.5$. The results for 200-mer and 300-mer solutions, with $q=0.4$ and 0.5, are collected in Table I. Note that capillary condensation will occur even for rather substantial undersaturations.

TABLE I. Capillary condensation results for 200-mers and 300-mers at solvent/monomer diameter ratios $q\equiv\sigma_s/\sigma_m$ being equal to 0.4 or 0.5. The bulk pressure is $\beta P_b\sigma_m^3=14.249\,55$, which is 5% higher than the bulk critical pressure at $N=200$ and $q=0.5$. Here $r\rho_p\sigma^3$ is the reduced monomer density in the bulk, while x_p is the corresponding polymer molar ratio, with index "sat" denoting its value at bulk coexistence (dilute branch). Finally, h_{cap} is the distance at which capillary condensation is predicted to occur under equilibrium conditions. For a polymer solution with 200-mers at $x_p/x_p^{\text{sat}}=0.7$ and $q=0.5$ no first-order transition was found: i.e., capillary condensation will under these conditions not occur. This system will display a continuous, rather than step wise, growth of the average polymer density in the slit as the surfaces are pushed closer together.

r	q	x_p/x_p^{sat}	$r\rho_p\sigma_m^3$	h_{cap}/σ_m
200	0.4	0.7	0.0002789	24.5
300	0.4	0.7	0.00001533	39.0
200	0.5	0.7	0.008909	N/A
200	0.5	0.9	0.01153	59.6
300	0.5	0.7	0.001606	34.9
300	0.5	0.8	0.001835	45.8
300	0.5	0.9	0.002063	76.2

Capillary condensation is driven by the attraction that the surfaces have to the monomers, induced by the smaller solvent particles. The regions of the condensed phase close to the center of the slit consist essentially of a metastable condensed phase, with an internal pressure, which is lower than the bulk pressure. This leads to a strong attraction between the surfaces, which are literally pushed together by the larger bulk pressure. The attractive condensed phase branch of the free energy is approximately linear in the vicinity of the transition, reflecting the approximately constant value for the internal pressure of the confined phase. The sudden onset of a strong attractive pressure, at separations where no depletion or bridging is expected, has also been measured experimentally in polymer solutions containing two different polymeric species[71] and microemulsions.[72] The authors proposed that the measured attractions were also due to capillary-induced phase transitions.

It is interesting to consider the structure of the dilute and concentrated phases. Examples of the density profiles for these phases are given in Fig. 4. The structure of the fluid density near the walls is very similar in the two phases for both the solvent and monomer species. In the dilute phase, however, the density profiles for both species approach their bulk values. In the concentrated phase, the density profiles approach their values on the metastable-concentrated branch of the bulk phase diagram. The appearance of the dilute phase is that of a thick film of polymer-rich phase close to the surface, which has an interface with the bulk solution phase in the center of the slit. This implies the existence of a surface transition at some lower polymer concentration. We shall investigate this conjecture in the next subsection.

As expected, we find that the larger the degree of undersaturation in the bulk, the smaller is the separation h_{cap} at which capillary condensation occurs. Figure 5 plots the average monomer density of the coexisting concentrated and dilute phases as a function of h_{cap} at various degrees of undersaturation in a solution of 300-mers with $q=0.5$. The two branches approach each other at large undersaturation, and

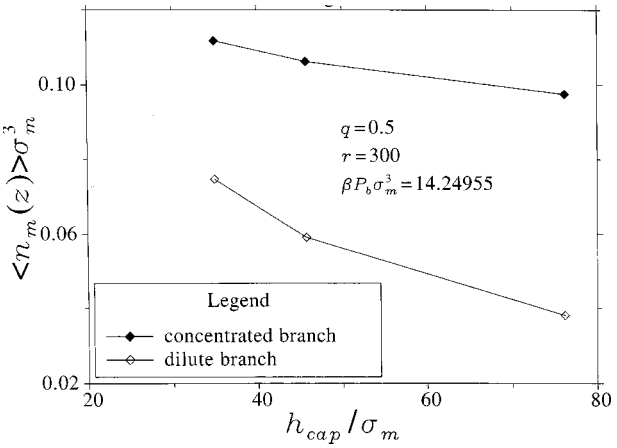

FIG. 5. Average monomer density in the slit at h_{cap}, which is the separation where the dilute and concentrated branches coexist. Data are shown for $x_p/x_p^{\text{sat}}=0.7$, 0.8, and 0.9.

the coexistence envelope will coalesce at some critical value. This behavior is analogous to the capillary critical separation found in single-component systems.[73,74] At undersaturations greater than the critical value, there is no longer a separation at which a transition of first order will occur. This is because h_{cap} has decreased to a value where the thick films in the dilute phase are not able to maintain separate interfaces. The films overlap and consequently are unable to form a phase distinct from the concentrated phase. Consistent with this is the observation that, in Fig. 5, the dilute phase branch approaches the concentrated branch.

In Fig. 6, we consider the surface free energy per unit area as a function of separation, in the presence of a bulk mixture containing 300-mers with $q=0.5$. The bulk pressure is again fixed at $\beta P_b\sigma_m^3=14.249\,55$, and we have investigated various values of undersaturation in the bulk. When $x_p/x_p^{\text{sat}}=0.7$, capillary condensation will occur at $h/\sigma_m \approx 35$, leading to a sudden increase of the attraction between the surfaces, for reasons that were discussed above. Both branches of the free energy curve are evident. As discussed

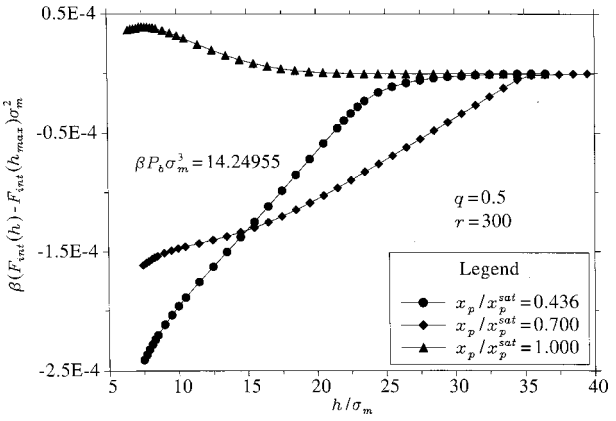

FIG. 6. (a) $\beta[F_{\text{int}}(h)-F_{\text{int}}(h_{\max})]\sigma_m^3$, where the latter term is the value of the net interaction free energy at the largest separation considered. Furthermore, $r=300$, $q=0.5$, and $\beta P_b\sigma_m^3=14.249\,55$. Circles, diamonds, and triangles are results for $x_p/x_p^{\text{sat}}=0.436$, 0.70, and 1.0. Only the stable solutions are given for $x_p/x_p^{\text{sat}}=0.70$, which displays a phase transition at $h/\sigma_m \approx 35$.

earlier, the approximately linear behavior of the free energy on the concentrated branch is typical of attractive interactions induced by capillary condensation. It is due to the presence of the thermodynamically metastable concentrated phase between the surfaces, which dominates the behavior at large separations. At shorter separations bridging interactions will act, whereby polymer molecules stretch between the surfaces, ''pulling'' them together.

At separations smaller than those shown in the Fig. 6, the free energy displays oscillatory behavior which is caused by hard sphere packing. At $x_p/x_p^{\text{sat}}\approx 0.436$, the bulk polymer solution is dilute enough to suppress capillary condensation. The free energy thus displays a single branch. Still, the rapidly increasing attraction at around $h/\sigma_m=25$ suggests that the system remains close to conditions which give rise to capillary condensation. However, at this degree of undersaturation the transition is not sharp, but has been ''smoothed out.'' As the surfaces approach each other, the thick films which form on either surface begin to overlap with a concomitant increase of the polymer density, although no sudden transition is evident.

At $x_p/x_p^{\text{sat}}=1.0$, the concentrated phase is stable at all separations, and the free energy curve displays a single branch. There is a repulsive barrier, due probably to the forced desolvation of the surfaces as they are pushed together. The interaction turns attractive at small separations, where bridging forces become important. Note that this repulsive barrier is present, even though strict equilibrium with a bulk solution is maintained at all separations. As such, it is completely unrelated to nonequilibrium effects caused by a slow diffusion of polymers, which sometimes is a serious problem in experimental situations. The ''thermodynamic'' barrier observed in this study may provide kinetic stabilization and in practice prevent flocculation of a colloidal dispersion.

2. Capillary-induced layering transitions

As described above, the *dilute* phase displays a thick film close to the surfaces. In this film, the polymer concentration is considerably higher than in the bulk. However, at even greater undersaturations than we have considered so far, a transition will occur to a dilute phase with a very thin film at the surfaces, in which the polymer density is only moderately higher than its bulk value. Examples of this surface layering transition will be considered at a bulk pressure of $\beta P_b\sigma_m^3=14.249\,55$. In order to simplify the notation, we shall refer to the layered phases as being respectively ''thin'' and ''thick.'' Layering transitions[75–78] are largely governed by packing effects and will only occur at very attractive surfaces. Contrary to prewetting, these transitions may take place at supercritical conditions. In our case, this corresponds to the bulk pressure being lower than its critical value. We denote by h_{tt} the separation at which thin and thick phases coexist in the slit.

Our results are collected in Table II. Here we have fixed the pressure and undersaturation of the bulk solution and varied the separation until there is coexistence between the thin and thick phases. Figure 7 shows an example of the interaction free energy per unit area as a function of separa-

TABLE II. Capillary induced layering transitions at hard walls in athermal polymer solutions, for two different bulk pressures (P_b), polymer lengths (N), and solvent/monomer diameter ratios ($q \equiv \sigma_s/\sigma_m$). The higher pressure is equal to $1.05P_b^c(N=200, q=0.5)$, while the lower is given by $1.05P_b^c(N=300, q=0.5)$, with P_b^c being the bulk critical pressure. h_{tt} is the separation at which thin and thick phases coexist.

r	q	$\beta P_b \sigma_m^3$	x_p/x_p^{sat}	h_{tt}/σ_m
200	0.5	14.24955	0.001	9.2
300	0.4	12.3837	0.0000001	7.9
300	0.4	12.3837	0.00000015	9.3
300	0.5	12.3837	0.045	20.5
300	0.5	14.24955	0.00008	12.5

tion for thin and thick phases. At large separations the thin phase is more stable than the thick phase. As the separation is decreased, the thick phase is stabilized by the presence of the other surface, causing its free energy to drop more steeply than that of the thin phase, and a crossover occurs at about $h/\sigma_m = 9.2$. Hence, if the surfaces are allowed to approach each other slowly from large separations, a capillary-induced transition will occur at about $h/\sigma_m = 9.2$, whereby thick films suddenly are formed at the surfaces. This transition will in turn give rise to a strong attraction between the surfaces. The reason that the layering transition happens at relatively short separations is most likely due to the extreme undersaturation, which gives rise to very narrow films. Thus, at large and intermediate separations, there is very little overlap between films at adjacent surfaces. However, at short separations, polymer molecules begin to benefit from the presence of the other surface by forming bridges and thereby lowering the free energy. This behavior is apparent in the density profiles shown in Fig. 8. The corresponding thin phases are not displayed, since the monomer densities are so low as to be undetectable on the same scale.

As we shall see below, polymer solutions with thick phases at the surfaces will display a much stronger and more long-ranged force than their thin phase counterparts. We can analyze this a bit further in terms of separate pressure contributions acting across the midplane of the slit. These can be

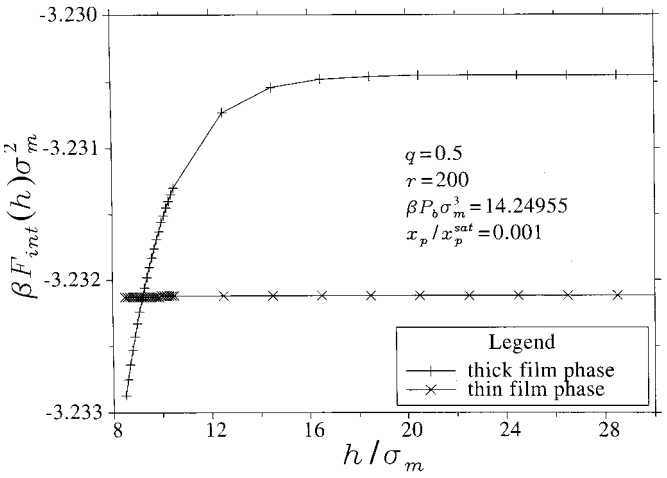

FIG. 7. Interaction free energies for the thick (+) and thin (×) branch in a 200-mer solution at $\beta P_b \sigma_m^3 = 14.249\,55$, where $q=0.5$ and $x_p/x_p^{\mathrm{sat}}=0.001$.

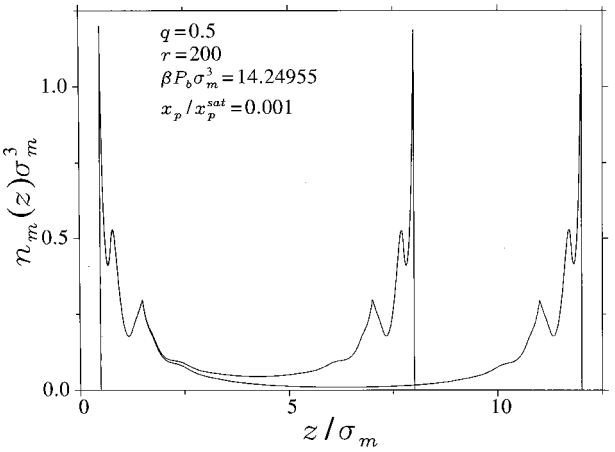

FIG. 8. Monomer density profiles in the thick phase at two different separations. Bulk conditions are identical to those specified in Fig. 7. The density enhancement at the midplane is obvious from the profile at the shorter separation.

subdivided into (i) an ideal pressure $\P_{\mathrm{id}}$, which is given by the sum of the monomer and solvent midplane densities, (ii) a collisional pressure P_{coll} due to hard core collisions transferring momentum across the midplane, and (iii) a bridging pressure due to connected monomers stretching across the midplane.

Since we are only interested in how these change with separation, we will subtract their value at infinite separation: i.e., we will only discuss $P_{\mathrm{id}}^*(h) = P_{\mathrm{id}}(h) - P_{\mathrm{id}}(\infty)$, etc. When thin phases are present at the surfaces in systems with $q<1$, P_{id}^* is generally repulsive, despite the existence of polymer depletion. As the larger monomers leave the slit, the volume they previously occupied is partly, but not quite, replaced by smaller solvent particles. The net effect is an increase of P_{id}^* and P_{br}^* and a decrease of P_{coll}^*. Normally, the latter dominates and we observe a weak attraction, but at high monomer concentrations, there is a repulsive barrier prior to the attraction at short separations. When there are thick phases at the surfaces, the monomer concentration *increases* as the separation is reduced, even at rather short separations. This induces a decreased density of the smaller solvent particles as well as of the total density. In this case, P_{id}^* and P_{br}^* are attractive, while P_{coll}^* is repulsive. The net pressure is strongly attractive, at least when the monomer concentration is low, and more long ranged than when thin phases are present. The observation of a strongly attractive regime at short separations in surface force experiments of polymer solutions is often attributed to depletion attraction. The results we present here suggest that this interpretation often is incorrect.

C. Influence of monomer size on surface forces

The presence of a thick polymer-rich phase at the surfaces has a dramatic effect on surface forces. By varying the monomer diameter relative to that of a fixed solvent diameter, we are able to modify the effective interaction between polymers and the surfaces. This allows us to control the fluid transitions which occur at or between the surfaces.

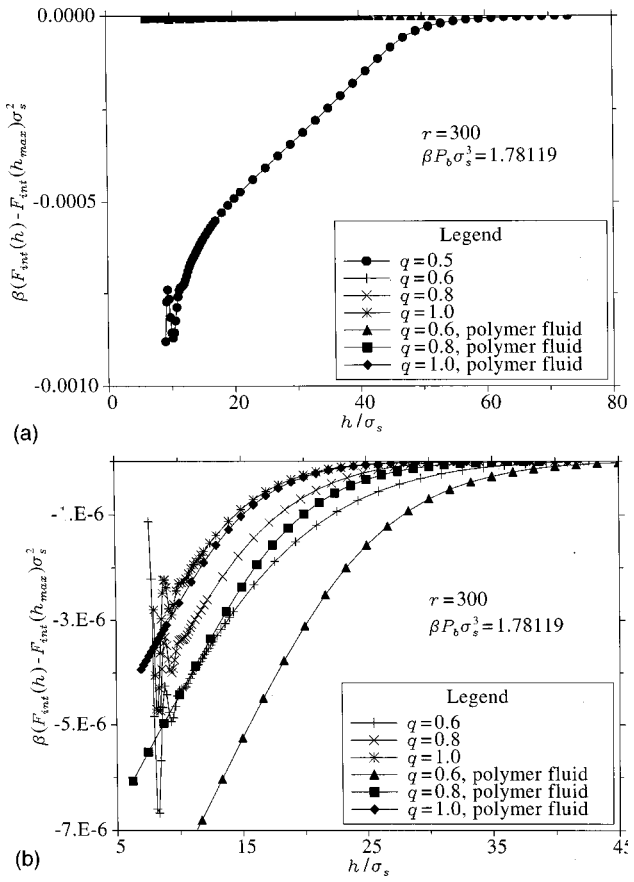

FIG. 9. σ_m dependence of surface forces for 300-mer solutions at $\beta P_b\sigma_s^3 \approx 1.781\,19$. Circles, plus signs, crosses, and stars are results at $q=0.5$, 0.6, 0.8, and 1.0. Pure polymer fluid results are denoted by triangles ($q=0.6$), squares ($q=0.8$), and diamonds ($q=1.0$). Here $h_{\max}$ is the largest separation, in each case, at which calculations have been made. Graph (b) is a blowup of the part of graph (a) which is relevant for $q=0.6$, 0.8, and 1.0.

In Fig. 9(a) we have collected results obtained when the monomer diameter is varied in a 300-mer solution, while maintaining a constant size of the solvent particles. The reduced bulk pressure is fixed at $\beta P_b\sigma_s^3=1.781\,193\,75$. As the monomer diameter is changing, it is appropriate to reduce the pressure by the solvent diameter σ_s. For $q=0.5$ this pressure corresponds to $\beta P_b\sigma_m^3=14.249\,55$. The bulk monomer density is fixed at $r\rho_p\sigma_s^3=0.000\,125$, which corresponds to $x_p/x_p^{\mathrm{sat}}\approx 0.436$ for $q=0.5$. The free energy curve for $q=0.5$ was presented earlier, though here we also include the structural oscillations at very short separations. The period of the oscillations is approximately equal to the monomer diameter. This indicates that the oscillatory force is due to polymer structuring in the thick layers at the surfaces and becomes apparent when the thick layers overlap at short separations. On the same scale, the interaction free energies at other monomer diameters ($q=0.6$–1.0) are insignificant. These systems display a stable thin phase at the surfaces in the entire separation regime we have investigated. In Fig. 9(b), the scale has been changed to make the free energy curves for $q=0.6$–1.0 more discernible. They show an attraction with oscillatory structure at short separations. The attraction is due to polymer depletion: i.e., surfaces restrict polymer configurations, making the environment unfavorable. Polymer molecules will tend to be depleted from the interstitial region. The reduction of the volume fraction dominates over the repulsion from an increased net density and a decrease of the attractive bridging terms. Consequently, the surfaces are pushed together by the surrounding bulk. The period of the short-ranged oscillatory structure is the same in all cases and is approximately equal to the solvent diameter. This indicates that the oscillatory forces are due to solvent structuring, which has a significant effect at short surface separations.

Also displayed in Fig. 9(b) are the results obtained for pure polymer fluids at the same bulk concentrations. The pure polymer fluid contains excluded volume effects and can be considered a crude polymer solution model, wherein the implicit solvent occupies the volume not taken up by the polymer. The polymer fluid model reproduces the depletion attraction reasonably well, although its range is overestimated, particularly at large monomer diameters. Solvent structuring effects are of course absent.

At $q=0.5$, the polymer fluid approach gives surface interactions which are several orders of magnitude smaller than those obtained when the solvent is explicitly included. The reason is that the formation of thick layers will only occur in the latter description, since they occur as a consequence of the surface affinity the monomers obtain due to their large size, as compared with the solvent particles.

We will end this section with a brief discussion on how the surface interactions respond to an increased polymer density. We have made some calculations at a polymer density corresponding to the concentrated branch of the bulk coexistence curve for a 300-mer solution at $\beta P_b\sigma_m^3=14.249\,55$. This means that the monomer density is $r\rho_p\sigma_s^3\approx 0.0104$. We will not present the results explicitly, but rather mention their qualitative features. Note, though, that the $q=0.5$ case is actually provided in Fig. 6 (with $x_p/x_p^{\mathrm{sat}}=1$). As mentioned previously, these conditions lead to a interaction curve in which there is a region of substantial repulsion prior to a rapidly growing attraction at short separations. This qualitative behavior is preserved at higher q values and also in the implicit solvent approach. However, when the size disparity is too small to admit a stable thick phase at the surfaces, the height of the repulsive barrier is reduced by more than an order of magnitude.

D. Influence of polymer length on surface forces

The polymer length is of course expected to significantly influence the surface forces. In Fig. 10 the interaction free energy per unit area is plotted for polymer solutions with $q=0.5$. Polymers of different lengths are compared at a fixed value of the bulk monomer concentration, $r\rho_p\sigma_m^3=0.001$. The bulk pressure is fixed at $\beta P_b\sigma_m^3=14.249\,55$. This means that x_p/x_p^{sat} is about 0.436 for the 300-mer solution and about 0.077 for the 200-mer solution, while the pressure is below critical for the 100-mer and 150-mer solutions. The 300-mer free energy is the same as in Fig. 6. We see a marked difference between this interaction and those obtained for the shorter chains. Furthermore, in the 100-mer solution, the thin phase solution is the stable one down to about h_{tt}/σ_m

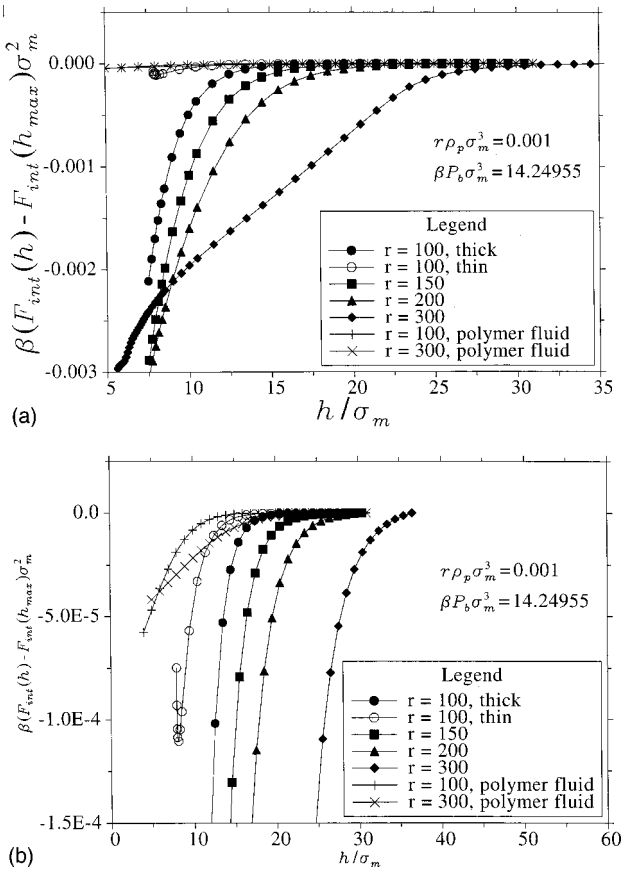

FIG. 10. Polymer length dependence of surface forces at $q=0.5$ and $\beta P_b\sigma_m^3 = 14.249\,55$. Here $h_{\max}$ is the largest separation considered, in each case. (a) Circles, squares, triangles, and diamonds are used for $r=100$, 150, 200, and 300-mer solutions. The 100-mer solution displays a thick branch (solid symbols), which is metastable above $h/\sigma_m \approx 7.9$. The corresponding (stable) thin branch is indicated by open symbols. Pure polymer fluid results are given for $r=100$ (+) and 300 (×). (b) A blowup showing details of the polymer fluid results and the thin phase branch of the 100-mer solution.

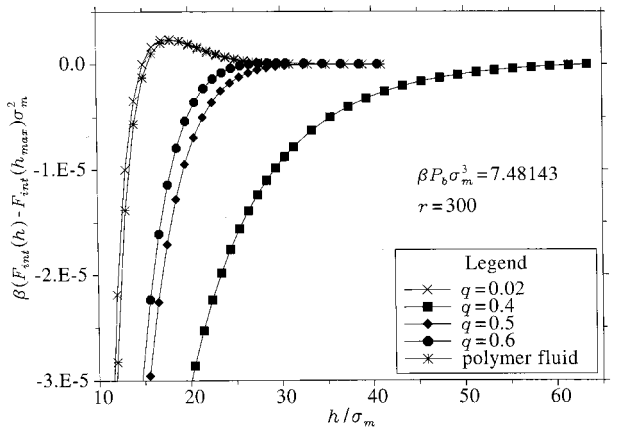

FIG. 11. σ_s dependence of surface forces for 300-mer solutions $\beta P_b\sigma_m^3 = 7.481\,43$. Here $h_{\max}$ is the maximum separation considered, in each curve. Crosses, squares, diamonds, circles, and stars are results for $q=0.02$, 0.4, 0.5, 0.6 and pure polymer fluid results.

$=7.9$, below which the thick phase is favored. Note that the thin phase diplays a repulsive regime near h_{tt}. This is most likely due to the onset of solvent structuring. As nonequilibrium effects are common and thus interesting in these systems, we have displayed both the thin and thick phase surface forces for $r=100$. The thick phase branch gives the interaction free energy that would be observed if the system remains in the metastable thick phase at all separations. For the other polymer lengths considered, the thick phase is stable at all separations. The surface force for the 300-mer solution has a much longer range than those of the shorter polymers. In addition, the free energy has a linear regime which, as discussed above, represents the smoothing-out of a capillary condensation effect.

In Fig. 10 we also show the results for the pure polymer fluid (implicit solvent). This model predicts weak depletion attraction forces for the corresponding polymer lengths and the given bulk monomer density. Hence the polymer fluid approach appears to be inappropriate for these systems. Even for the 100-mer solution, within the separation regime where the thin phase is stable, there are significant discrepancies between the two levels of description, although the agreement is naturally much better than in cases where the polymer solution displays a stable thick phase.

E. Influence of the solvent diameter on surface forces

We now consider the influence of the solvent diameter on the surface forces. The pressure is held fixed at $\beta P_b\sigma_m^3 = 7.481\,43$. In addition, the bulk monomer concentration is fixed at $r\rho_p\sigma_m^3 = 0.01$. In Fig. 11, we observe attractions in all cases. The range of the attraction increases with decreasing q. The attraction is due to the polymer bridging which is strengthened upon reducing q, due to the increase in monomer surface attractions. However, when the solvent diameter is very small, $q=0.02$, the depletion attraction between monomers and the surfaces is reduced to essentially zero. In this case, the solution results is very close to the those for the implicit solvent approach. Here we see a repulsive barrier in the free energy, with an attraction at shorter range, due to polymer depletion.

F. Pressure dependence of surface forces

In this section we will consider the effect of bulk pressure on surface forces. In particular, we consider two pressures $\beta P_b\sigma_m^3 = 7.481\,43$ and $11.676\,06$, while the polymer length is fixed at $r=300$. Furthermore, $q=0.5$ and the bulk polymer concentration is $r\rho_p\sigma_m^3 = 0.01$. At the lower pressure, the monomer density at the surfaces displays a depleted profile. Here excluded volume effects, which drive the positive adsorption of monomers to the surfaces, are small. Instead, the configurational entropy loss the polymers experience near the surfaces dominates, which leads to a decreased monomer density in these regions. This is illustrated in Figs. 12(a) and 12(b). At the higher pressure, the monomer adsorption at the walls is enhanced. Indeed, it is apparent that thick films have formed at the surfaces, as is clear from Fig. 12(b). The formation of the films has a significant effect on the surface interactions: see Fig. 13. The dependence on bulk pressure, as observed in this example, cannot be reproduced by the implicit solvent model. This model depends only on the bulk polymer density, which is again held fixed at

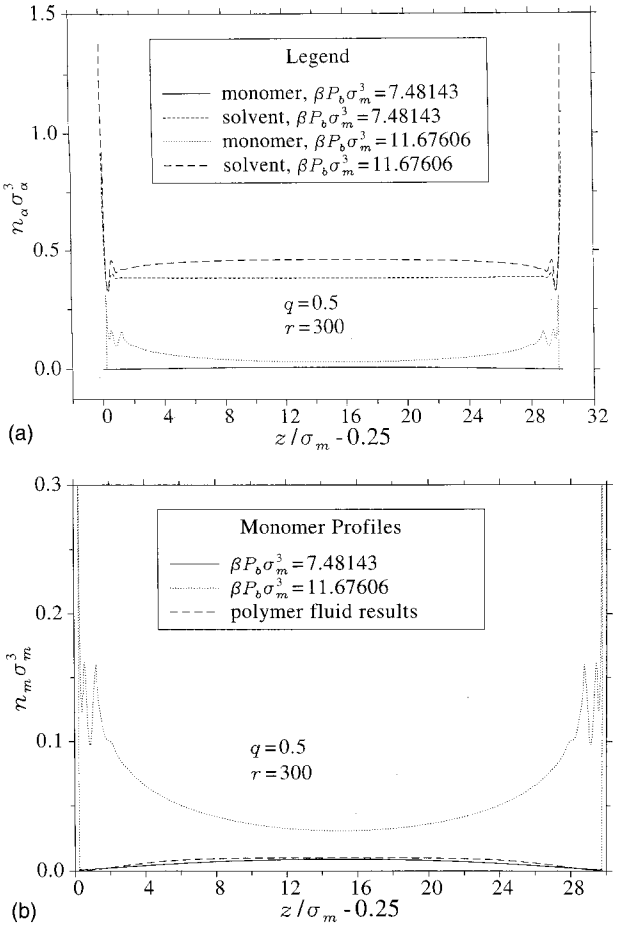

FIG. 12. Density profiles in a 300-mer solution with $q=0.5$. Thin solid lines are used for results at $\beta P_b\sigma_m^3 = 7.481\,43$, while thick solid ones denote results obtained at a higher pressure, $\beta P_b\sigma_m^3 = 11.676\,06$. The dashed curve gives the density profile of the corresponding pure polymer fluid. (a) Solvent and monomer density profiles. (b) Details of the monomer density profiles.

$r\rho_p\sigma_m^3 = 0.01$. At this density the monomer profiles display a typical depleted form, with the concomitant depletion attraction observed in the surface interactions. The implicit solvent approach predicts that the attractive pressure levels off to a constant value at short separations. This simply reflects the fact the polymer density in the slit has shrunk to a negligible value.

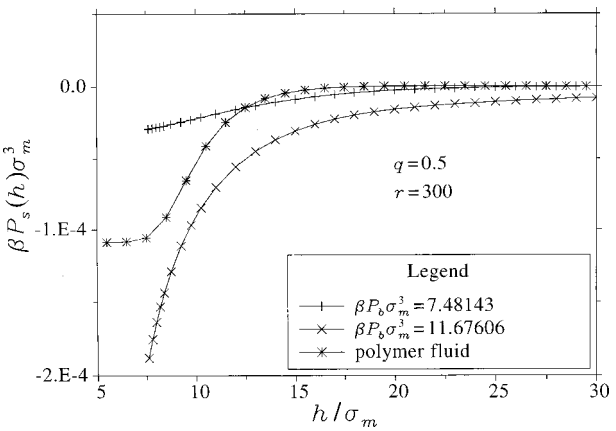

FIG. 13. Net interaction pressure results in a 300-mer solution with $q=0.5$, at $\beta P_b\sigma_m^3 = 7.481\,43$ (+) and $\beta P_b\sigma_m^3 = 11.676\,06$ (×). Stars are used for pure polymer fluid results.

IV. CONCLUSIONS

We have shown that the extended-GFD functional is able to reproduce demixing in a bulk fluid. This transition manifests itself as a capillary demixing (''condensation'') between surfaces. The transition is driven by a size disparity between monomers and the solvent, which leads to an effective attraction between monomer particles. Capillary condensation to a polymer-rich phase is brought about by a further effective attraction between monomers and the hard surfaces, mediated by the smaller solvent molecules. This phase transition leads to a sudden attraction between the surfaces. In addition, our functional predicts the existence of a surface layering transition, which is also capable of strongly affecting surface interactions.

According to our findings, the implicit solvent approach (pure polymer fluid) is able to predict the the general features of surface forces, provided no thick films are formed at the surfaces if the solvent is included explicitly. In the latter case, the discrepancy between the two approaches is severe and even more so if capillary condensation occurs at some separation.

Note that thick phases appears to be stable even at very large undersaturations—i.e., for a considerable range of different conditions. Hence they may well be a very important ingredient among the factors that regulate for instance the stability of colloidal dispersions, where polymers are present. This is especially likely considering that our findings have been made in athermal systems, with only hard sphere interactions. The existence of, for example, an monomer adsorbing potential at the surfaces would naturally increase the propensity for the system to display a stable polymer-rich thick phase near these. This would be true even if each solvent particle were equally attracted to the surfaces, since cooperativity effects would lead to a stronger adsorption of monomers. We are currently studying how the presence of adsorbing potentials affects the surface forces in these systems, and the results will be presented shortly.

ACKNOWLEDGMENTS

One of the authors (J.F.) gratefully acknowledges financial support by the Swedish Foundation for International Cooperation in Research and Higher Education.

[1] S. S. Patel and M. Tirrell, Annu. Rev. Phys. Chem. **40**, 597 (1989).
[2] H.-W. Hu and S. Granick, Macromolecules **23**, 613 (1990).
[3] M. Ruths, H. Yoshizawa, L. J. Fetters, and J. N. Israelachvili, Macromolecules **29**, 7193 (1996).
[4] T. Kuhl *et al.*, Langmuir **12**, 3003 (1996).
[5] A. L. Ogden and J. A. Lewis, Langmuir **12**, 3413 (1996).
[6] T. Kuhl, S. Berman, Alan D. Wen Hui, and J. N. Israelachvili, Macromolecules **31**, 8250 (1998).
[7] T. Kuhl, S. Berman, Alan D. Wen Hui, and J. N. Israelachvili, Macromolecules **31**, 8258 (1998).
[8] M. Seitz, C. K. Park, J. Y. Wong, and J. N. Israelachvili, Langmuir **17**, 4616 (2001).
[9] S. Asakura and F. Oosawa, J. Chem. Phys. **22**, 1255 (1954).
[10] S. Asakura and F. Oosawa, J. Polym. Sci. **33**, 183 (1982).

[11] A. Vrij, Pure Appl. Chem. **48**, 471 (1976).
[12] J.-F. Joanny, L. Leibler, and P. G. de Gennes, J. Polym. Sci., Polym. Phys. Ed. **17**, 1073 (1979).
[13] B. Vincent, P. F. Luckham, and F. Waite, J. Colloid Interface Sci. **73**, 508 (1980).
[14] P. G. de Gennes, Macromolecules **14**, 637 (1982).
[15] P. G. de Gennes, Macromolecules **15**, 492 (1982).
[16] R. I. Feigin and D. H. Napper, J. Colloid Interface Sci. **74**, 567 (1980).
[17] R. I. Feigin and D. H. Napper, J. Colloid Interface Sci. **75**, 525 (1980).
[18] G. J. Fleer and J. M. H. Scheutjens, Croat. Chem. Acta **60**, 477 (1987).
[19] C. E. Woodward, J. Chem. Phys. **97**, 695 (1992).
[20] Y. Mao, M. E. Cates, and H. N. W. Lekkerkerker, Phys. Rev. Lett. **75**, 4548 (1995).
[21] A. N. Semenov and J.-F. Joanny, Europhys. Lett. **29**, 279 (1995).
[22] J. Bonet-Avalos, J.-F. Joanny, A. Johner, and A. N. Semenov, Europhys. Lett. **35**, 97 (1996).
[23] A. Broukhno, T. Åkesson, B. Jönsson, and P. Vorontsov-Velyaminov, J. Phys. Chem. **113**, 1 (2000).
[24] A. Czezowski, Ph.D. thesis, ADFA, Canberra, 2001.
[25] J. Walz and A. Sharma, J. Colloid Interface Sci. **168**, 485 (1994).
[26] D. Chandler, J. D. McCoy, and J. S. Sherwin, J. Chem. Phys. **85**, 5971 (1986).
[27] W. E. McMullen and K. F. Freed, J. Chem. Phys. **92**, 1413 (1990).
[28] C. E. Woodward, J. Chem. Phys. **94**, 3183 (1991).
[29] J. V. Selinger and R. F. Bruinsma, Phys. Rev. A **43**, 2910 (1991).
[30] E. Kierlik and M. L. Rosinberg, J. Chem. Phys. **97**, 9222 (1992).
[31] E. Kierlik and M. L. Rosinberg, J. Chem. Phys. **99**, 3950 (1993).
[32] J. D. McCoy, K. G. Honell, K. S. Schweizer, and J. D. Curro, J. Chem. Phys. **95**, 9348 (1991).
[33] E. Kierlik and M. L. Rosinberg, J. Chem. Phys. **100**, 1716 (1992).
[34] C. E. Woodward and A. Yethiraj, J. Chem. Phys. **100**, 3181 (1994).
[35] A. Yethiraj and C. E. Woodward, J. Chem. Phys. **102**, 5499 (1995).
[36] A. Yethiraj, J. Chem. Phys. **109**, 3269 (1998).
[37] S. Nordholm, M. Johnson, and B. C. Freasier, Aust. J. Chem. **33**, 2139 (1980).
[38] D. J. Tildesley and W. B. Street, Mol. Phys. **41**, 85 (1980).
[39] K. G. Honell and C. K. Hall, J. Chem. Phys. **90**, 1841 (1989).
[40] K. G. Honell and C. K. Hall, J. Chem. Phys. **95**, 4481 (1991).
[41] A. Yethiraj, J. D. Curro, K. S. Scweizer, and J. D. McCoy, J. Chem. Phys. **98**, 1635 (1993).
[42] J. M. Wichert, H. S. Gulati, and C. K. Hall, J. Chem. Phys. **105**, 7669 (1996).
[43] Y. C. Chiew, Mol. Phys. **70**, 129 (1990).
[44] Y. Song, S. M. Lambert, and J. M. Prausnitz, Macromolecules **27**, 441 (1994).
[45] J. Chang and S. I. Sandler, J. Chem. Phys. **103**, 3196 (1995).
[46] R. J. Sadus, Macromolecules **29**, 7212 (1996).
[47] I. H. Kim and Y. C. Bae, Fluid Phase Equilibria **168**, 201 (2000).
[48] T. Biben and J. P. Hansen, Phys. Rev. Lett. **66**, 2215 (1991).
[49] T. Biben and J. P. Hansen, J. Phys.: Condens. Matter **3**, F65 (1991).
[50] H. N. W. Lekkerkerker and A. Stroobants, Physica A **195**, 387 (1993).
[51] Y. Rosenfeld, Phys. Rev. Lett. **72**, 3831 (1994).
[52] M. Dijkstra and D. Frenkel, J. Chem. Phys. **101**, 3179 (1994).
[53] W. C. K. Poon and P. B. Warren, Europhys. Lett. **28**, 513 (1994).
[54] A. D. Dinsmore, A. G. Yodh, and D. J. Pine, Phys. Rev. E **52**, 4045 (1995).
[55] A. D. Dinsmore, P. B. Warren, W. C. K. Poon, and A. G. Yodh, Europhys. Lett. **40**, 337 (1997).
[56] M. Dijkstra, R. van Roij, and R. Evans, Phys. Rev. Lett. **81**, 2268 (1998).
[57] D. Henderson, D. Bode, K.-Y. Chang, and D. T. Wasan, Mol. Phys. **95**, 131 (1998).
[58] M. Dijkstra, R. van Roij, and R. Evan, Phys. Rev. E **59**, 5744 (1999).
[59] P. Bartlett and R. H. Ottewill, Phys. Rev. E **63**, 021504 (2001).
[60] P. Bartlett, R. H. Ottewill, and P. P. N , Phys. Rev. Lett. **68**, 3801 (1992).
[61] J. S. van Duijneveldt, A. W. Heinen, and H. N. W. Lekkerkerker, Europhys. Lett. **21**, 369 (1993).
[62] P. D. Kaplan, J. L. Rouke, A. G. Yodh, and D. J. Pine, Phys. Rev. Lett. **72**, 582 (1994).
[63] A. Imhof and J. K. G. Dhont, Phys. Rev. Lett. **75**, 1662 (1995).
[64] J. L. Lebowitz and J. S. Rowlinson, J. Chem. Phys. **41**, 133 (1964).
[65] J. A. Anta *et al.*, J. Chem. Phys. **106**, 2712 (1997).
[66] P. D. Guirati, Phys. Rev. E **63**, 021504 (2001).
[67] T. Boublik, Mol. Phys. **27**, 1415 (1974).
[68] J. N. Israelachvili, *Intermolecular and Surface Forces*, 2nd ed. (Academic Press, London, 1991).
[69] F. A. Escobedo and J. K. C. Suen, Mol. Phys. **89**, 1773 (1996).
[70] J. K. C. Suen, F. A. Escobedo, and J. J. de Pablo, J. Chem. Phys. **106**, 1288 (1997).
[71] Wennerström, Håkan, K. Thuresson, P. Linse, and E. Freyssingeas, Langmuir **14**, 5664 (1998).
[72] P. Petrov, U. Olsson, Wennerström, and Håkan, Langmuir **13**, 3331 (1997).
[73] R. Evans, M. Bettolo Marconi, and P. Tarazona, J. Chem. Phys. **84**, 2376 (1986).
[74] J. Forsman and C. E. Woodward, Mol. Phys. **90**, 637 (1997).
[75] J. H. Singleton and G. D. Halsey, J. Chem. Phys. **58**, 1011 (1954).
[76] Y. Lahrer, J. Chem. Phys. **72**, 1847 (1968).
[77] P. C. Ball and R. Evans, J. Chem. Phys. **89**, 4412 (1988).
[78] J. Forsman and C. E. Woodward, Mol. Phys. **90**, 189 (1999).